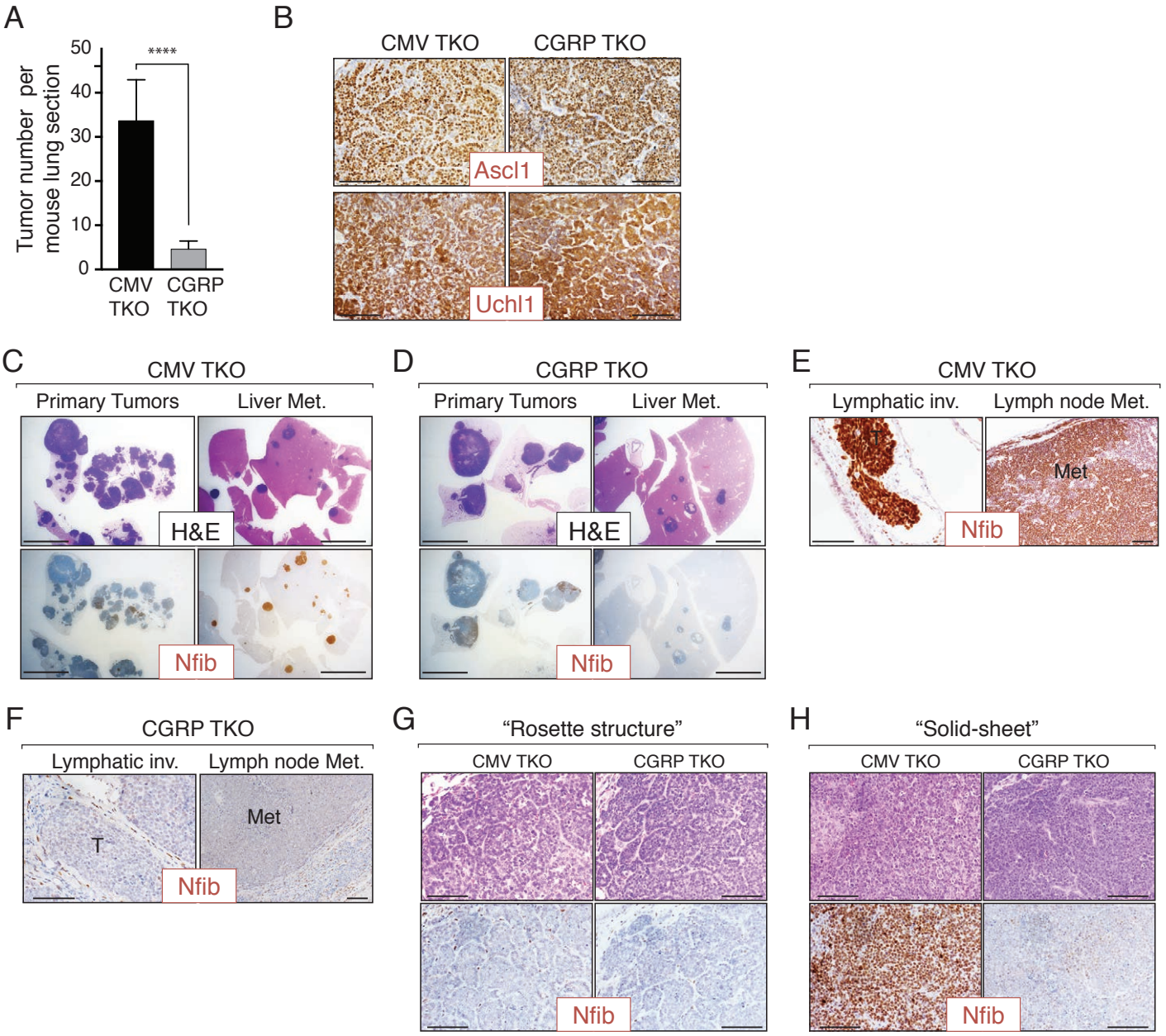

Figure S1: SCLC metastases in CMV TKO and CGRP TKO mice differ in Nfib expression.
A. Quantification of tumor number in CMV TKO (N=13) and CGRP TKO (N=19) mice. $p < 0.0001$, t - test.
B. SCLC tumors from both the CMV TKO and CGRP TKO models express the neuroendocrine markers Ascl1 and Uchl1. Scale bars = 100 μm.
C-D. Low magnification images of lung and liver. H&E staining (top) and Nfib immunostaining (bottom) are shown for representative CMV TKO **(C)** and CGRP TKO **(D)** primary tumors and metastases. Rare primary tumors/areas in both CMV TKO and CGRP TKO mice are $Nfib^{positive}$. The majority of the metastases in CMV TKO mice are $Nfib^{positive}$, while most of the metastases in CGRP TKO mice are $Nfib^{low/negative}$. Scale bars = 4 mm.
E-F. Nfib immunostaining of lymphatic invasion and lymph node metastases in CMV TKO and CGRP TKO mice. Lymphatic invasion and metastases in CMV TKO mice are mostly Nfib high, while lymphatic invasion and metastases inCGRP TKO mice are mostly $Nfib^{low/negative}$. Scale bars = 100 μm.
G-H. Rosette growth pattern areas (**G**) are characteristic of primary tumors in CMV TKO mice (5/5 mice examined) but also seen in the lungs of one CGRP TKO mouse (N=7 mice examined). Rosette growth pattern areas were not found in metastases (0/7 in CMV TKO mice and 0/5 in CGRP TKO mice). The solid-sheet growth pattern (**H**) was found in all primary tumors and metastases in both in CMV TKO and CGRP TKO mice. Rosette growth pattern areas in CMV TKO and CGRP TKO mice are $Nfib^{low/negative}$. Solid-sheet areas in CMV TKO mice are mostly $Nfib^{positive}$, while in CGRP TKO mice they are $Nfib^{low/negative}$. Scale bars = 100 μm.

A

Paper	Mouse Genotype	Cre	Experiments and Results
Dooley *et al.* Genes and Development 2011	*Rb1*$^{f/f}$;*p53*$^{f/f}$	Ad-CMV-Cre	- Copy number analysis on metastases and metastasis-derived cell lines (Fig. 2) Tumor: 7/15 (47%) Met: 9/13 (63%) - Immunohistochemistry for Nfib (Fig. S7) 75% of LN mets are Nfib^{high}, 90% of Liver mets are Nfib^{high}. Comment: **Nfib is highly expressed in CMV DKO metastases**
Wu *et al.* Oncotarget, 2016	*Rb1*$^{f/f}$;*p53*$^{f/f}$ *Rb1*$^{f/f}$;*p53*$^{f/f}$;*Pten*$^{f/+}$ *Rb1*$^{f/f}$;*p53*$^{f/f}$;*Pten*$^{f/f}$	Ad-CMV-Cre Ad-CMV-Cre Ad-CGRP-Cre	- Copy number analysis on metastases (Fig. 1) *Rb1*$^{f/f}$;*p53*$^{f/f}$ CMV-Cre: 5/9 Nfib amplified; *Rb1*$^{f/f}$;*p53*$^{f/f}$;*Pten*$^{f/+}$ CMV-Cre: 5/6 Nfib amplified *Rb1*$^{f/f}$;*p53*$^{f/f}$;*Pten*$^{f/f}$ CGRP-Cre: 0/2 Nfib not amplified - Nfib expression by qPCR in *Rb1*$^{f/f}$;*p53*$^{f/f}$ and *Rb1*$^{f/f}$;*p53*$^{f/f}$;*Pten*$^{f/+}$, both transduced by CMV-Cre 11/17 Nfib high expression Comment: **Nfib is highly expressed in CMV DKO and CMV Rb/p53/Pten$^{f/+}$ metastases.**

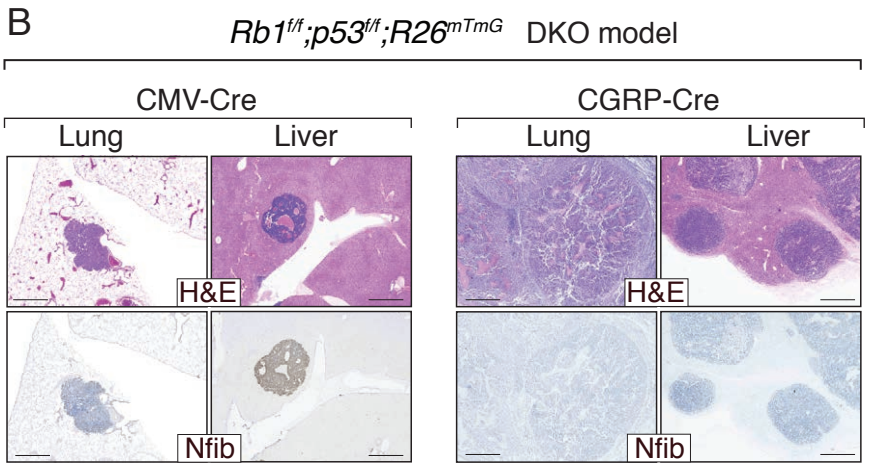

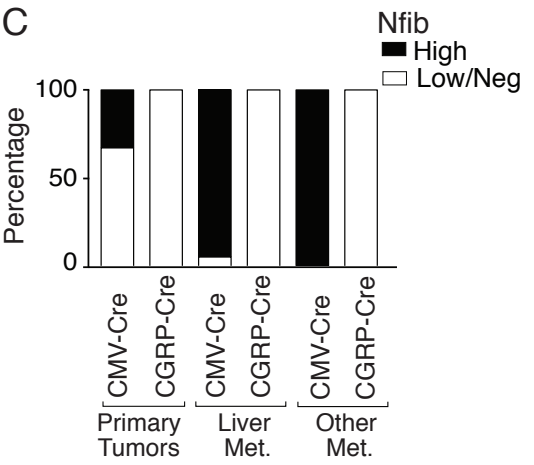

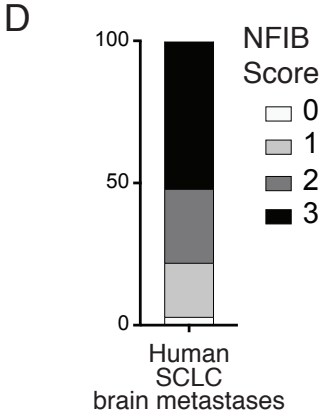

E

Paper	Method	Result
Semenova *et al.* Cell Report, 2016	Immuno-histochemistry	8/11 (73%) metastases were NFIB high
Hodgkinson *et al.* Nature Med, 2014	Copy number analysis	0/4 CDX models had *NFIB* amplification
Denny, Yang *et al.* Cell, 2016	Immuno-histochemistry	11/20 (55%) metastases were NFIB high
Dooley *et al.* Genes and Development, 2011	Copy number analysis	7/17 (41%) metastases derived cell lines had *NFIB* amplification

Figure S2: Expression of NFIB in mouse and human SCLC metastases.
A. Summary of published reports on Nfib expression in SCLC metastases from different genetically engineered mouse models.
B. Representative H&E and immunostaining images of SCLC tumors from CMV DKO (*Rb1*$^{f/f}$;*p53*$^{f/f}$;*R26*^{mTmG}) and CGRP DKO mice. Immunostaining for Nfib on primary tumors (Lung) and liver metastases (Liver) is shown. Scale bars = 1 mm.
C. Quantification of Nfib expression in the DKO models. CMV DKO primary tumors (N=30 tumors from 6 mice), CMV DKO liver metastases (N=509 metastases from 9 mice), CMV DKO other metastases (N=4 lymph node metastases from 2 mice), CGRP DKO primary tumors (N=5 tumors from 2 mice), CGRP DKO liver metastases (N=9 metastases from 1 mouse), and CGRP DKO other metastases (N=8 kidney and adrenal gland metastases from 1 mouse).
D. Quantification of NFIB expression in human SCLC brain metastases (scoring is shown in Fig. 1F).
E. Summary of published reports on NFIB amplification and expression in human SCLC metastases and xenografts derived from circulating tumor cells. Scoring and data for Nfib expression from Denny, Yang *et al.* are used in the analysis shown in Fig. 1F,G.

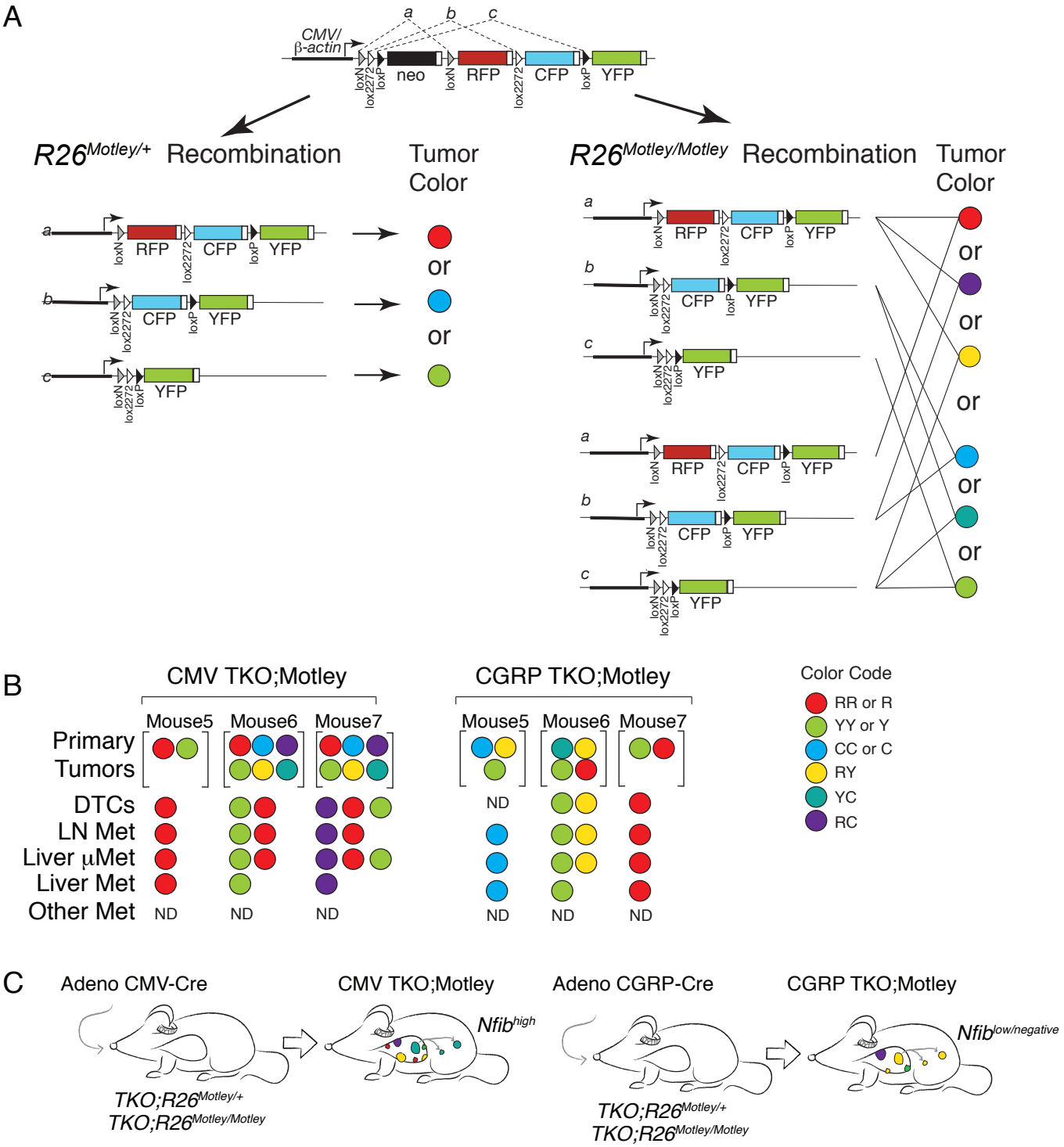

Figure S3: Multicolor tumor labeling in the CMV and CGRP SCLC models documents that not all large tumors gain the ability to disseminate and metastasize.

A. Schematic of the *Motley* allele and the potential outcomes of Cre-mediated recombination. Mice that are heterozygous for the *Motley* allele can generate tumors of 3 different colors while mice homozygous for the *Motley* allele can generate tumors of 6 different colors.

B. Summary of results from additional CMV TKO;Motley and CGRP TKO;Motley mice. The colors of the largest primary tumors, disseminated tumors cells (DTCs), and metastases are shown. μMet, micrometastases. ND, not detected.

C. Schematic of tumor progression in CMV TKO and CGRP TKO mice. In each mouse, with either CMV-Cre- or CGRP-Cre-initiated SCLC, metastases are predominantly only one color, therefore they are most likely given rise by a single tumor. As in CMV TKO;R26mTmG mice the metastases in CMV TKO;Motley mice were most often Nfib^{high} while metastases in CGRP TKO;Motley mice were Nfib$^{low/negative}$.

A

	Sample	Type	ATAC -seq	RNA -seq	Batch	Genotype by PCR *Rb1*	*p53*	*p130*
CGRP TKO	G1T1	Primary	x	x	2	Δ/Δ	Δ/Δ	Δ/*f*
	G1T2	Primary	x	x	2	Δ/Δ	Δ/Δ	Δ/Δ
	G2T1	Primary	x	x	2	Δ/Δ	Δ/Δ	Δ/Δ
	G2T2	Primary	x	x	2	Δ/Δ	Δ/Δ	Δ/Δ
	G2L1	Metastasis	x	x	2	Δ/Δ	Δ/Δ	Δ/Δ
	G2L2	Metastasis	x	x	2	Δ/Δ	Δ/Δ	Δ/Δ
	G3T1	Primary	x	x	2	Δ/Δ	Δ/Δ	Δ/Δ
	G3T2	Primary	x	x	2	Δ/Δ	Δ/Δ	Δ/Δ
	G3L2	Metastasis	x	x	2	Δ/Δ	Δ/Δ	Δ/Δ
	G3L3	Metastasis	x	x	2	Δ/Δ	Δ/Δ	Δ/Δ
	G6T1	Primary	x	x	2	Δ/Δ	Δ/Δ	Δ/Δ
	G6T2	Primary	x	x	2	Δ/Δ	Δ/Δ	Δ/Δ
	G6L1	Metastasis	x	x	2	Δ/Δ	Δ/Δ	Δ/Δ
	G6L2	Metastasis	x	x	2	Δ/Δ	Δ/Δ	Δ/Δ
	G6L3	Metastasis	x	x	2	Δ/Δ	Δ/Δ	Δ/Δ
	G5T1	Primary	x		3	nd	nd	nd
	G5T2	Primary	x		3	nd	nd	nd
CMV TKO	DY2T1	Primary		x	4	Δ/Δ	Δ/Δ	Δ/Δ
	DY2T2	Primary		x	4	Δ/Δ	Δ/Δ	Δ/Δ
	DY2T3	Primary		x	4	Δ/Δ	Δ/Δ	Δ/Δ
	DY2N1	Metastasis		x	4	Δ/Δ	Δ/Δ	Δ/Δ
	DY2L1	Metastasis		x	4	Δ/Δ	Δ/Δ	Δ/Δ
	DY2L2	Metastasis		x	4	Δ/Δ	Δ/Δ	Δ/Δ
	DY5T1	Primary		x	4	Δ/Δ	Δ/Δ	Δ/Δ
	DY5T2	Primary		x	4	Δ/Δ	Δ/Δ	Δ/Δ
	DY5T4	Primary		x	4	Δ/Δ	Δ/Δ	Δ/Δ
	DY5N1	Metastasis		x	4	Δ/Δ	Δ/Δ	Δ/Δ
	DY5L1	Metastasis		x	4	Δ/Δ	Δ/Δ	Δ/Δ
	DY5L2	Metastasis		x	4	Δ/Δ	Δ/Δ	Δ/Δ
	DY53T1	Primary		x	4	Δ/Δ	Δ/Δ	Δ/Δ
	DY53T2	Primary		x	4	Δ/Δ	Δ/Δ	Δ/Δ
	DY53T3	Primary		x	4	Δ/Δ	Δ/Δ	Δ/Δ
	DY53N1	Metastasis		x	4	Δ/Δ	Δ/Δ	Δ/Δ
	DY53L1	Metastasis		x	4	Δ/Δ	Δ/Δ	Δ/Δ
	DY53Lm	Metastasis		x	4	Δ/Δ	Δ/Δ	Δ/Δ
	DY4T1	Primary		x	4	Δ/Δ	Δ/Δ	Δ/Δ
	DY4T2	Primary		x	4	Δ/Δ	Δ/Δ	Δ/Δ
	DY4T4	Primary		x	4	Δ/Δ	Δ/Δ	Δ/Δ
	DY11T2	Primary		x	4	Δ/Δ	Δ/Δ	Δ/Δ
	DY11T3	Primary		x	4	Δ/Δ	Δ/Δ	Δ/Δ
	DY11N1	Metastasis		x	4	Δ/Δ	Δ/Δ	Δ/Δ
	DY9T1	Primary		x	4	Δ/Δ	Δ/Δ	Δ/Δ
	DY9T2	Primary		x	4	Δ/Δ	Δ/Δ	Δ/Δ
	DY9N1	Metastasis		x	4	Δ/Δ	Δ/Δ	Δ/Δ
	DY9Lm	Metastasis		x	4	Δ/Δ	Δ/Δ	Δ/Δ
	V1T1	Primary	x		1	nd	nd	nd
	V1L1	Metastasis	x		1	nd	nd	nd
	V2T1	Primary	x		1	nd	nd	nd
	V2L1	Metastasis	x		1	nd	nd	nd
	V3T1	Primary	x		1	nd	nd	nd
	V3L1	Metastasis	x		1	nd	nd	nd
	V4T1	Primary	x		1	nd	nd	nd
	V4L1	Metastasis	x		1	nd	nd	nd
	V5T1	Primary	x		3	nd	nd	nd
	V5T2	Primary	x		3	nd	nd	nd
	V5T3	Primary	x		3	nd	nd	nd
	V5T4	Primary	x		3	nd	nd	nd
	V5N1	Metastasis	x		3	nd	nd	nd
	V5L1	Metastasis	x		3	nd	nd	nd
	V5L2	Metastasis	x		3	nd	nd	nd

B

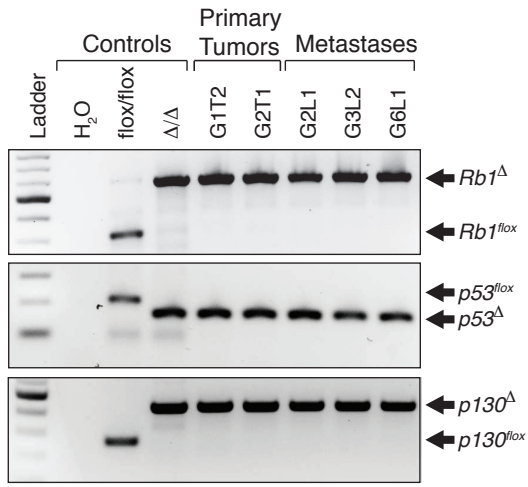

Figure S4: Tumor samples from CMV TKO and CGRP TKO mice for ATAC-seq and RNA-seq analyses.
A. Samples used for ATAC-seq and RNA-seq analysis are marked with an "x". The batch in which each sample was analyzed is indicated and the RNA-seq and ATAC-seq samples were corrected for batch effects (see Methods). For all samples used for RNA-seq, we also extracted DNA and used it for PCR genotyping of the floxed *Rb1, p130*, and *p53* alleles. nd = no data. ATAC-seq sample from CMV TKO mice are from Denny, Yang *et al*, 2016.
B. PCR genotyping gel of representative tumor samples.

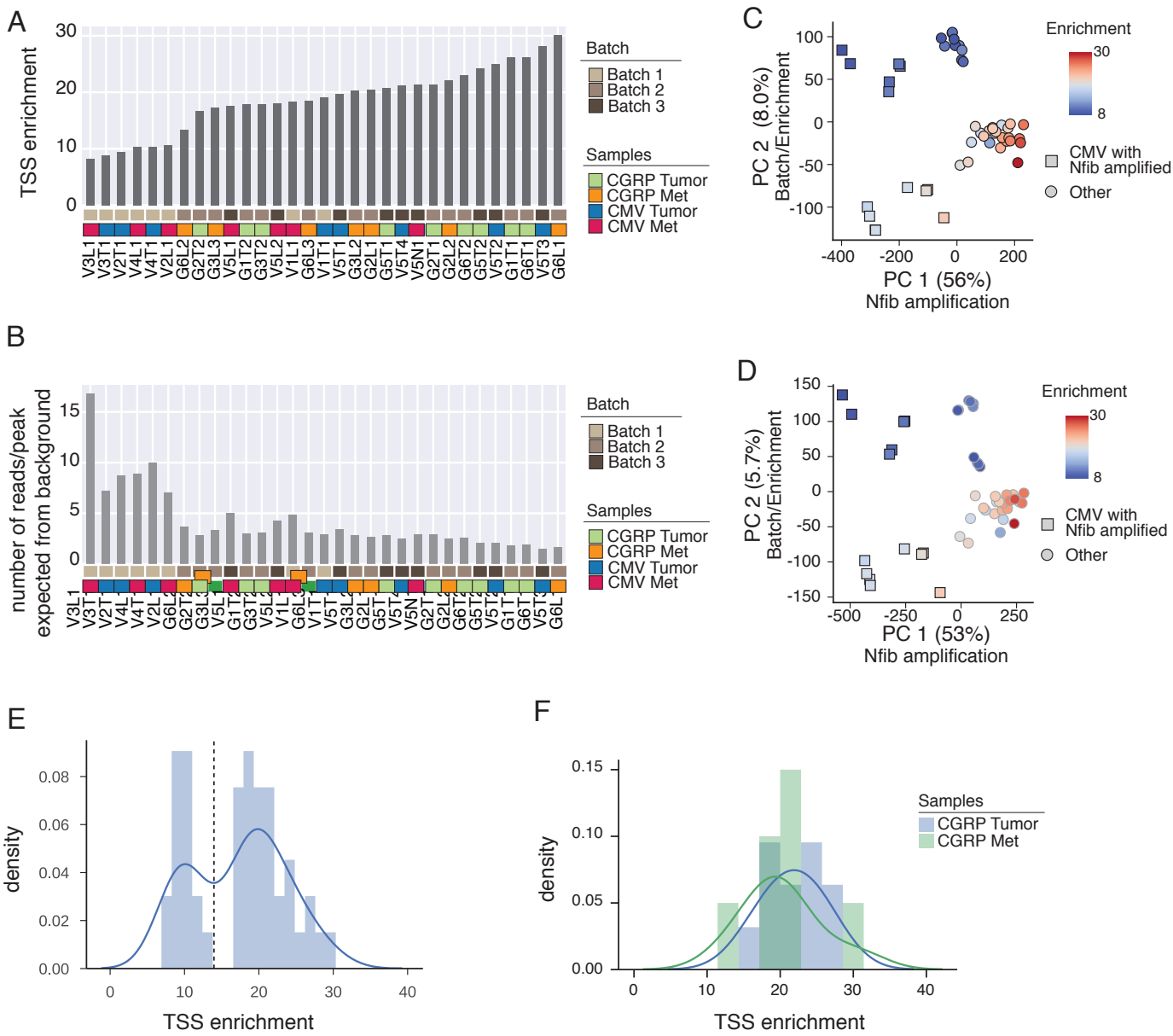

Figure S5: TSS enrichment analysis and removal of samples with poor enrichment score.
A. Variability in TSS enrichment in ATAC samples, which roughly corresponds to different batches of samples that were processed more than a year apart.
B. Variability in the number of reads/peak expected from background fragmentation, normalized across samples for sequencing depth.
C-D. Principal component analysis (PCA) of the sequencing depth-normalized, regularized log counts within accessible regions, either raw counts (**C**) or after subtracting reads expected from background fragmentation (**D**). Differences in enrichment are associated with large differences in accessibility (i.e. PC2), even after subtracting reads expected from background fragmentation.
E. To reduce variability due to low background fragmentation, samples with an enrichment score less than 14 were not included in the analysis to identify differentially accessible regions.
F. TSS enrichment of CGRP tumors and metastases. CGRP tumors and metastases do not have significantly different enrichment scores.

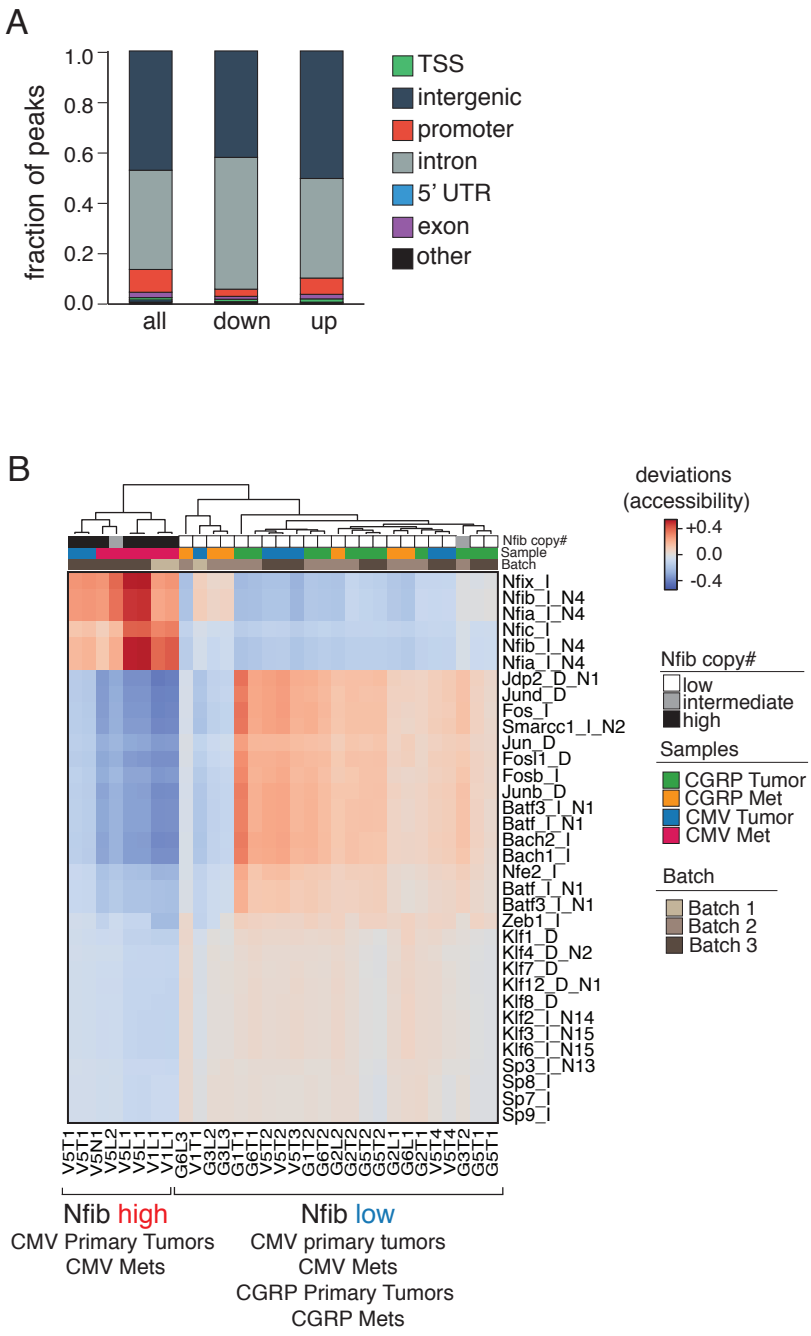

Figure S6: Regions with decreased chromatin accessibility in CGRP TKO metastases compared to primary tumors are enriched for bZIP factor motifs.

A. Location of genomic regions with increased (up) and decreased (down) chromatin accessibility in CGRP TKO metastases.

B. Heatmap of differential enriched motif in differentially accessible regions in CGRP tumors and metastases as well as enrichment for Nfi motifs in CMV Nfib^{high} samples across all samples (TSS enrichment > 14) from CMV TKO and CGRP TKO mice.

C. HOMER *de novo* motif enrichments in regions with decreased accessibility in CGRP TKO metastases relative to CGRP TKO primary tumors identified motifs most similar to bZIP and Tbx20 transcription factor binding motifs.

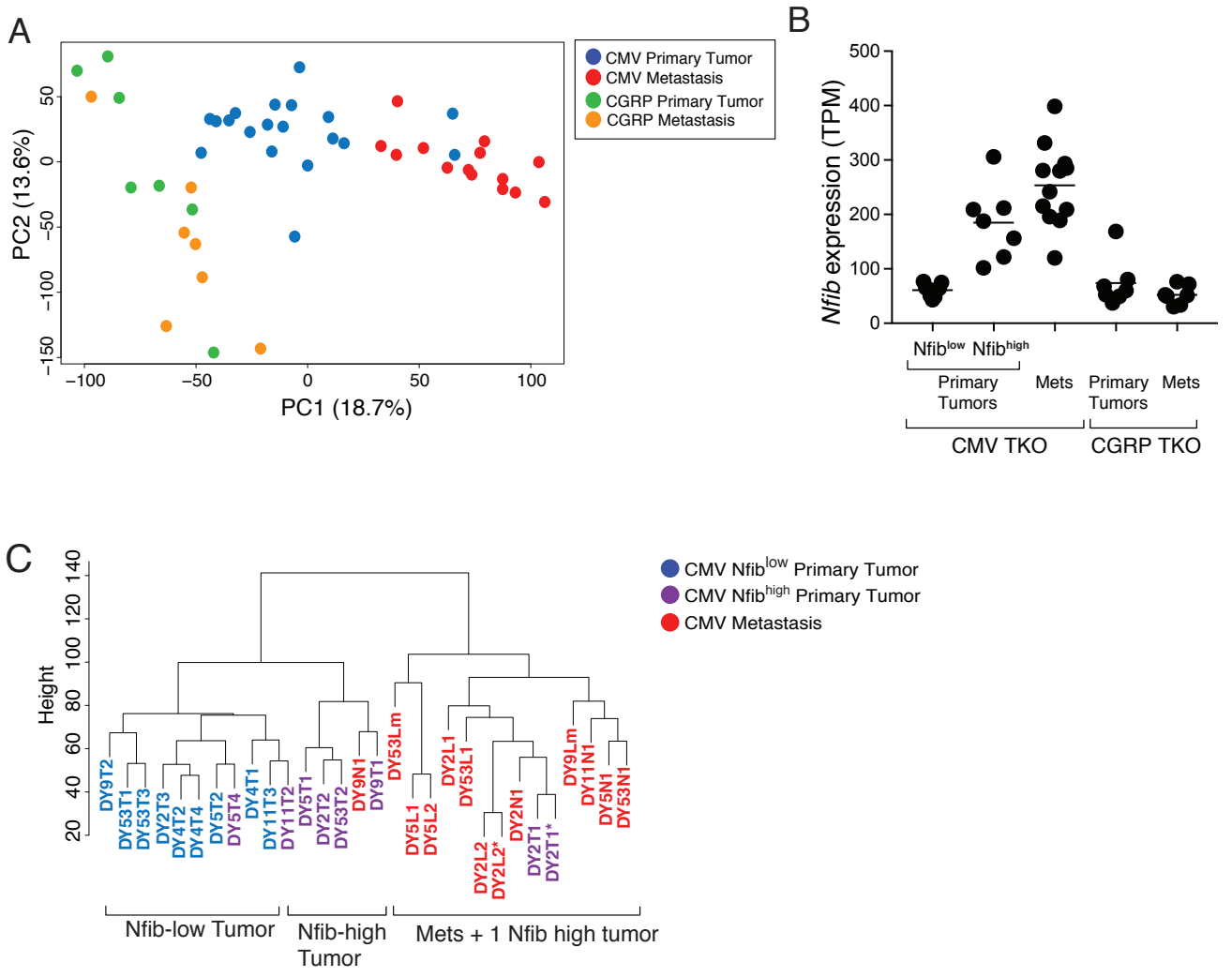

Figure S7: Molecularly distinct SCLC subtypes.
A. Principal component analysis (PCA) on gene expression of tumors and metastases from CMV TKO and CGRP TKO mice after batch correction.
B. Nfib mRNA expression in primary tumors and metastases from CMV TKO and CGRP TKO mice. CMV TKO primary tumors can be binned into Nfib^{high} (TPM > 100) and Nfib^{low} groups (TPM < 100).
C. Unsupervised hierarchical clustering of CMV TKO primary tumors and metastases. Nfib^{high} primary tumors cluster with CMV TKO metastases.

A

GO term enriched in CMV metastases: sister chromatids segregation

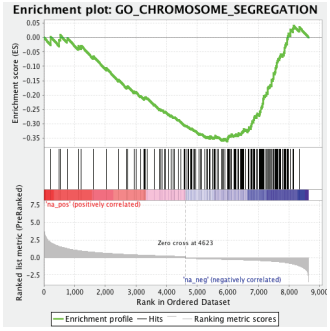

NES = -2.19, FDR = 6E-3

B

GO term enriched in CMV metastases: Spinal Cord motor neuron differentiation

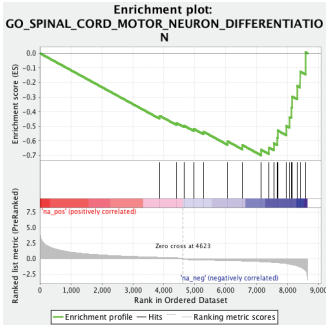

NES = -2.42, FDR = 4E-4

C

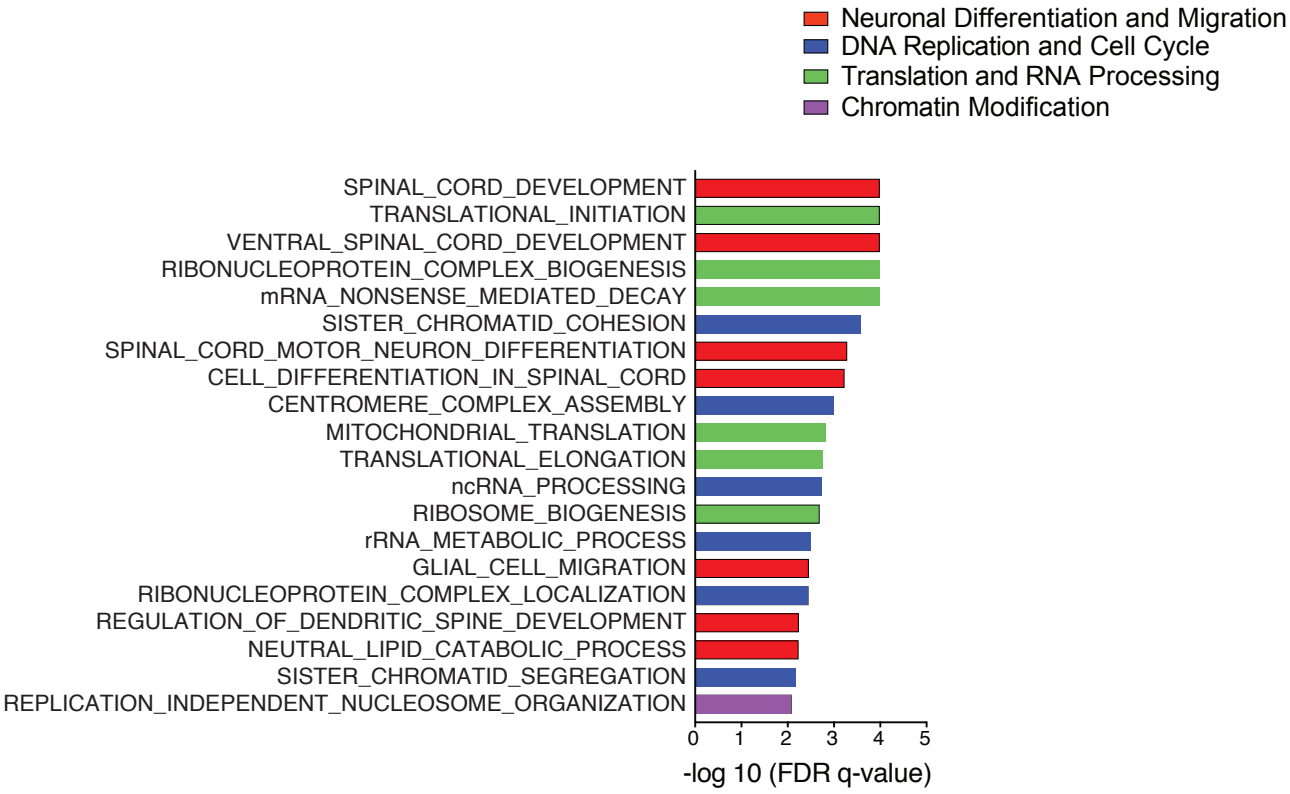

Figure S8: CMV TKO metastases are enriched for cell cycle and neuronal differentiation programs.
A. Gene set enrichment analysis (GSEA) of gene ontology (GO) enriched for chromosome segregation in CMV TKO metastases in comparison to CMV Nfib^{low} primary tumors.
B. GSEA plot of GO enriched for spinal cord / neuronal differentiation in CMV TKO metastases in comparison to CMV Nfib^{low} primary tumors.
C. Top 20 GO terms with smallest FDR q value in CMV TKO metastases in comparison to CMV Nfib^{low} primary tumors.

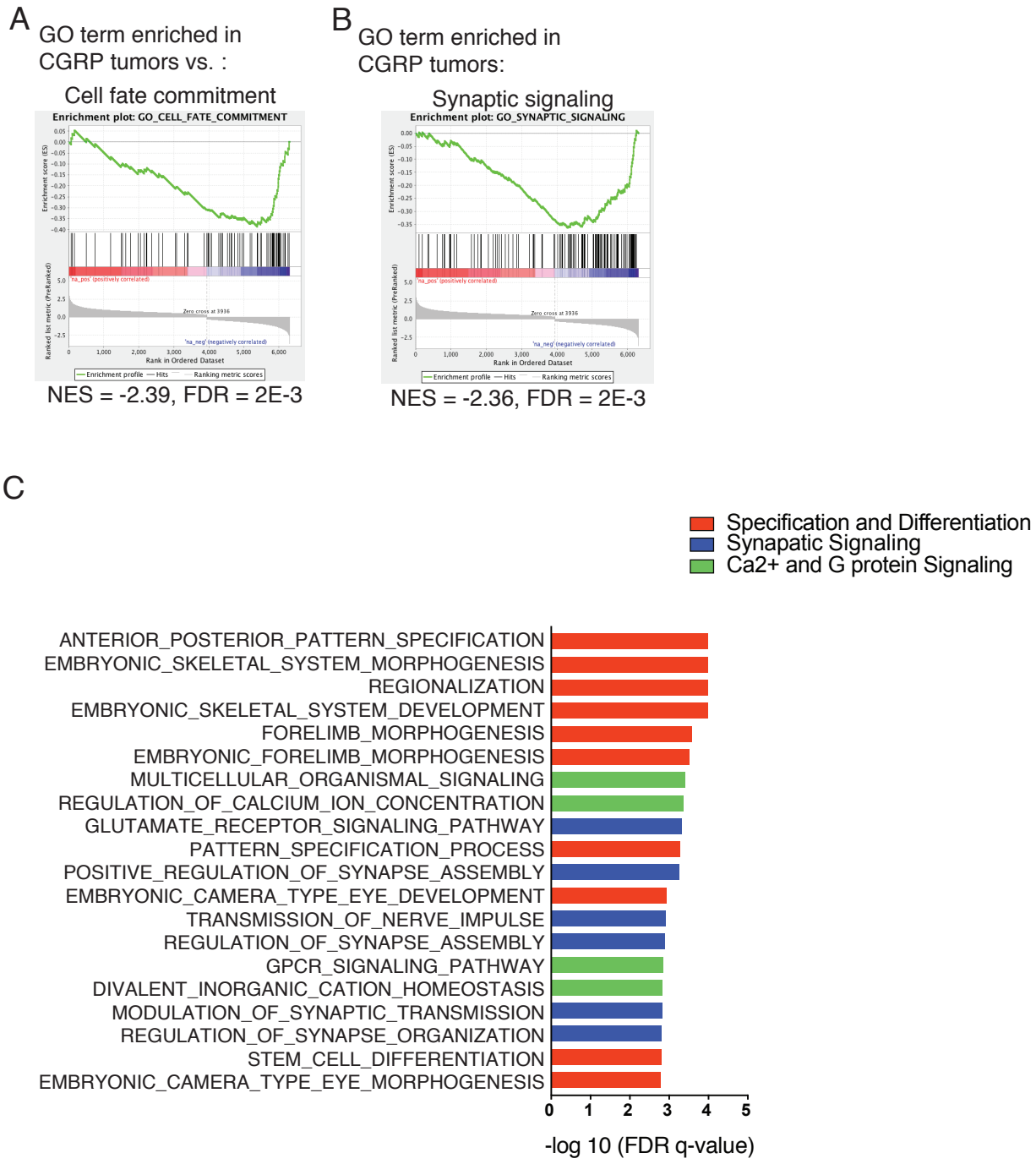

Figure S9: CGRP TKO primary tumors have a more mature neuronal gene expression signature.
A. Gene set enrichment analysis (GSEA) of gene ontology (GO) enriched for cell fate commitment in CGRP TKO tumors in comparison to CMV Nfib^{low} primary tumors.
B. Gene set enrichment analysis (GSEA) of gene ontology (GO) enriched for synaptic signaling in CGRP TKO tumors in comparison to CMV Nfib^{low} primary tumors.
C. Top 20 GO terms with smallest FDR q value in CGRP TKO tumors in comparison to CMV Nfib^{low} primary tumors.

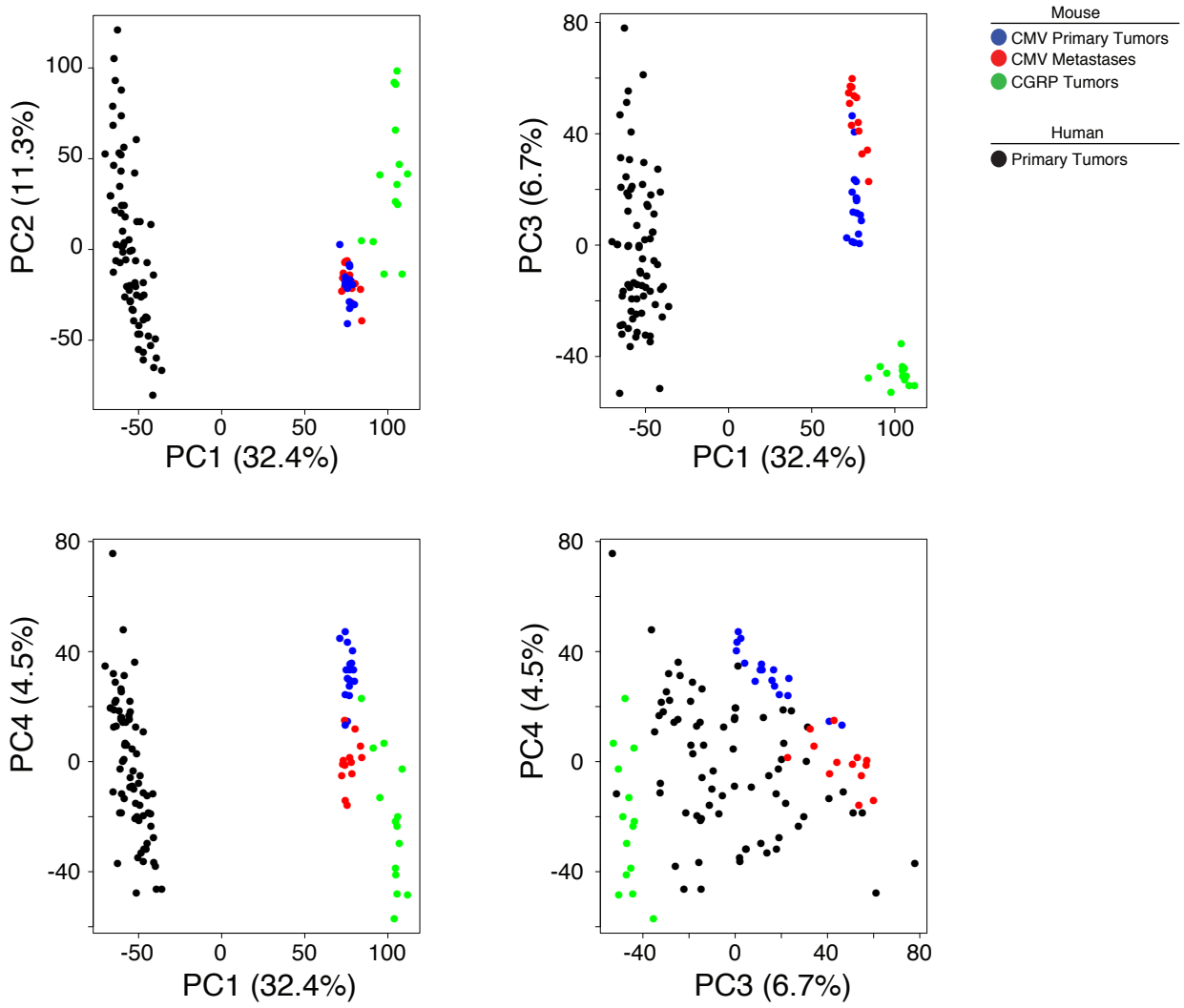

Figure S10: Human SCLC tumors have gene expression programs that are diverse and encompass both CMV TKO and CGRP TKO tumors.
Principal component analysis of human SCLC tumors and the SCLC tumors from the CMV TKO and CGRP TKO models. Principal component 1 (PC1) is driven by species. Across the other major principal components human tumors are distributed broadly with some being more similar to CGRP TKO tumors and other being more similar to CMV TKO tumors. To show the relationship between the human and mouse SCLC samples in a manner that does not include the dominant PC1, we also show PC3 versus PC4. This analysis highlights the distribution of human SCLC between the CMV TKO and CGRP TKO states.

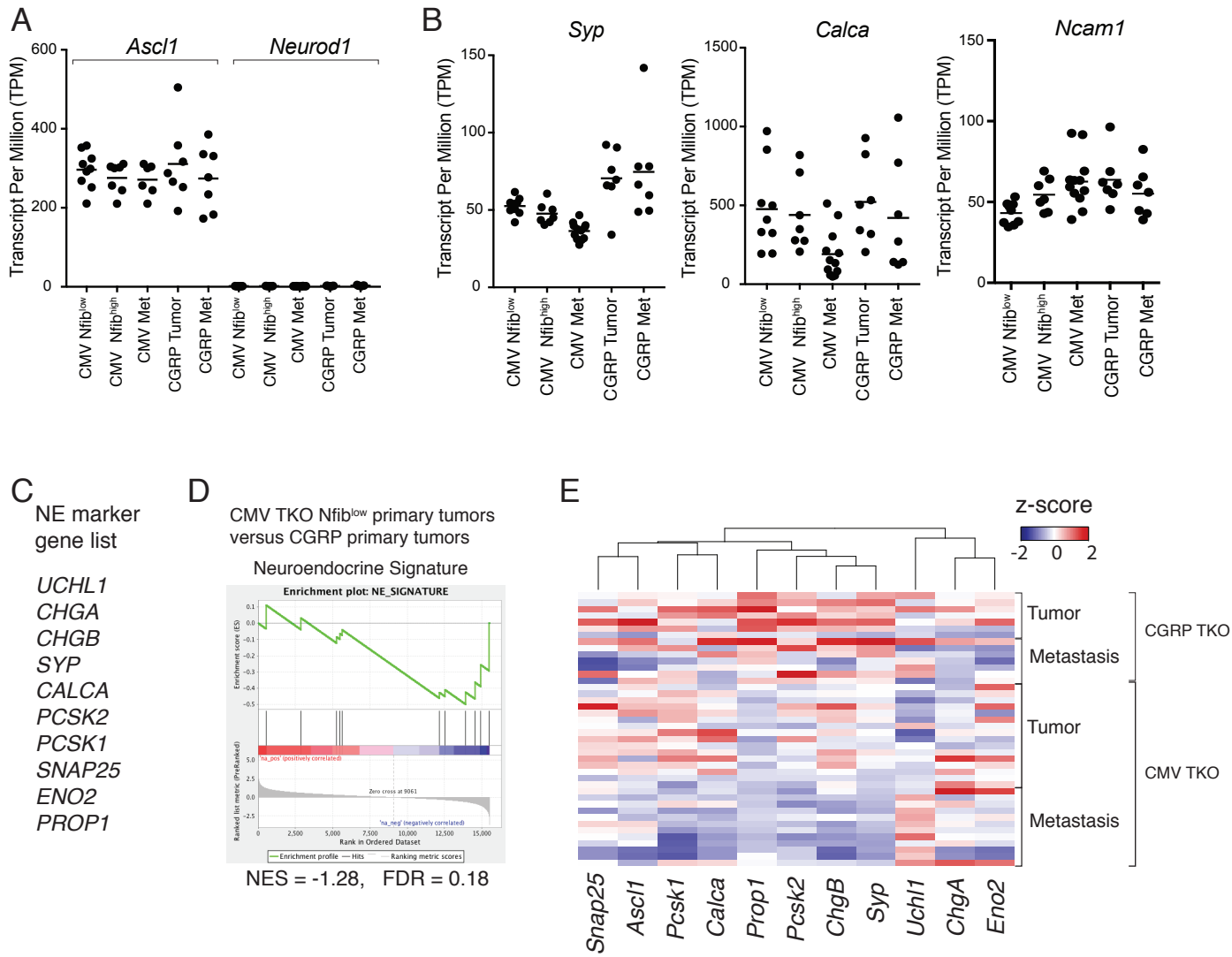

Figure S11: CGRP TKO tumors are more neuroendocrine than CMV TKO tumors, while CMV TKO tumors highly express multiple markers of different lung epithelium lineages compared to CGRP TKO tumors.
A. Ascl1 and Neurod1 RNA expression in CMV TKO and CGRP TKO tumors (TPM from RNA-seq data). All CMV TKO and CGRP TKO tumors are Ascl1^{high}, Neurod1^{low}.
B. Both CMV TKO and CGRP TKO tumors and metastases hgihly expresses neuroendocrine markers, including Syp, Calca and Ncam1.
C. A list of neuroendocrine genes used for the neuroendocrine gene signature geneset (From Endocrine Pathology vol 14.).
D. Gene set enrichment analysis (GSEA) showed a slight enrichment of neuroendocrine gene signatures in CGRP TKO primary tumors compared to CMV TKO Nfib^{low} primary tumors.
E. Heatmap of z-score showing gene expression of neuroendocrine markers. CGRP TKO primary tumors have higher expression of several neuroendocrine markers compared to CMV TKO tumors.

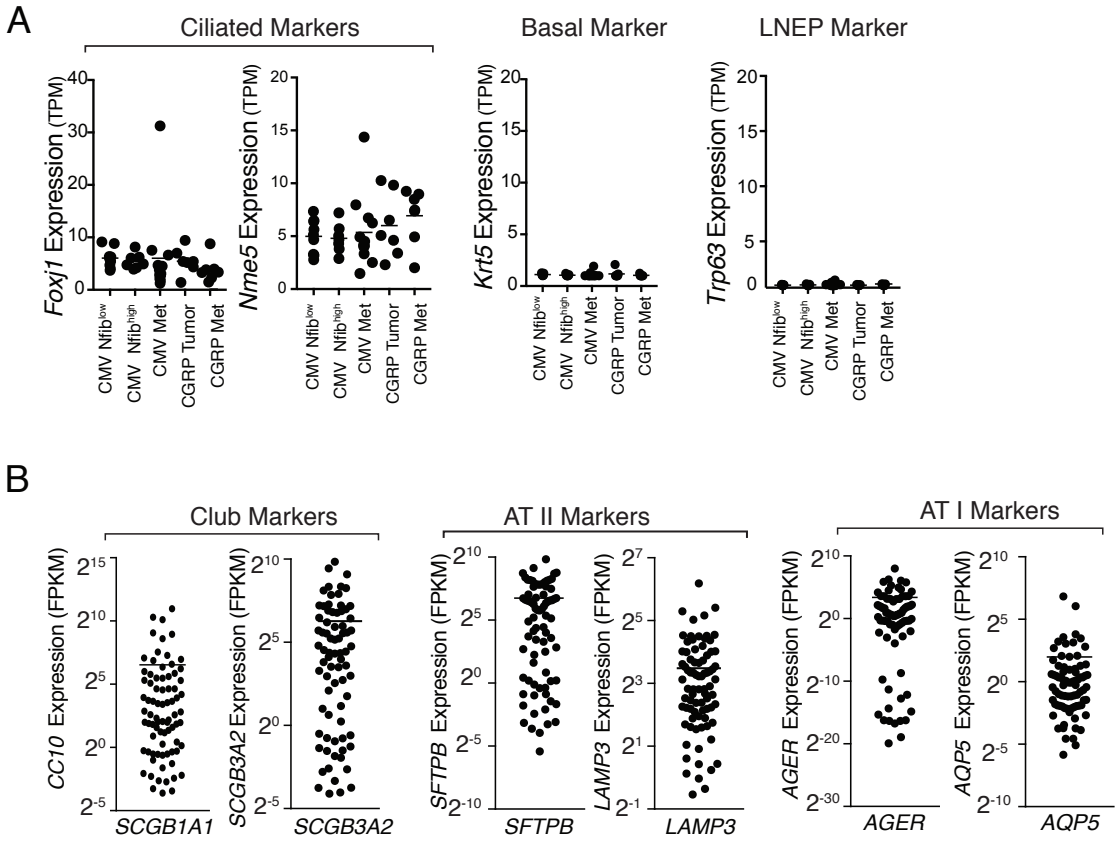

Figure S12: Expression of multilineage genes in SCLC tumors.
A. Expression of markers of different lung epithelium lineages in tumors and metastases from CMV TKO and CGRP TKO mice. None of the tumors express high levels of ciliated, basal, or LNEP/DASC cell markers.
B. Expression of markers of different lung epithelium lineages in human SCLC tumors (data from George, Lim *et al.* 2015). A fraction of human SCLC tumors highly express multiple markers of different lung epithelium lineages. Note $\log_2$ scale.

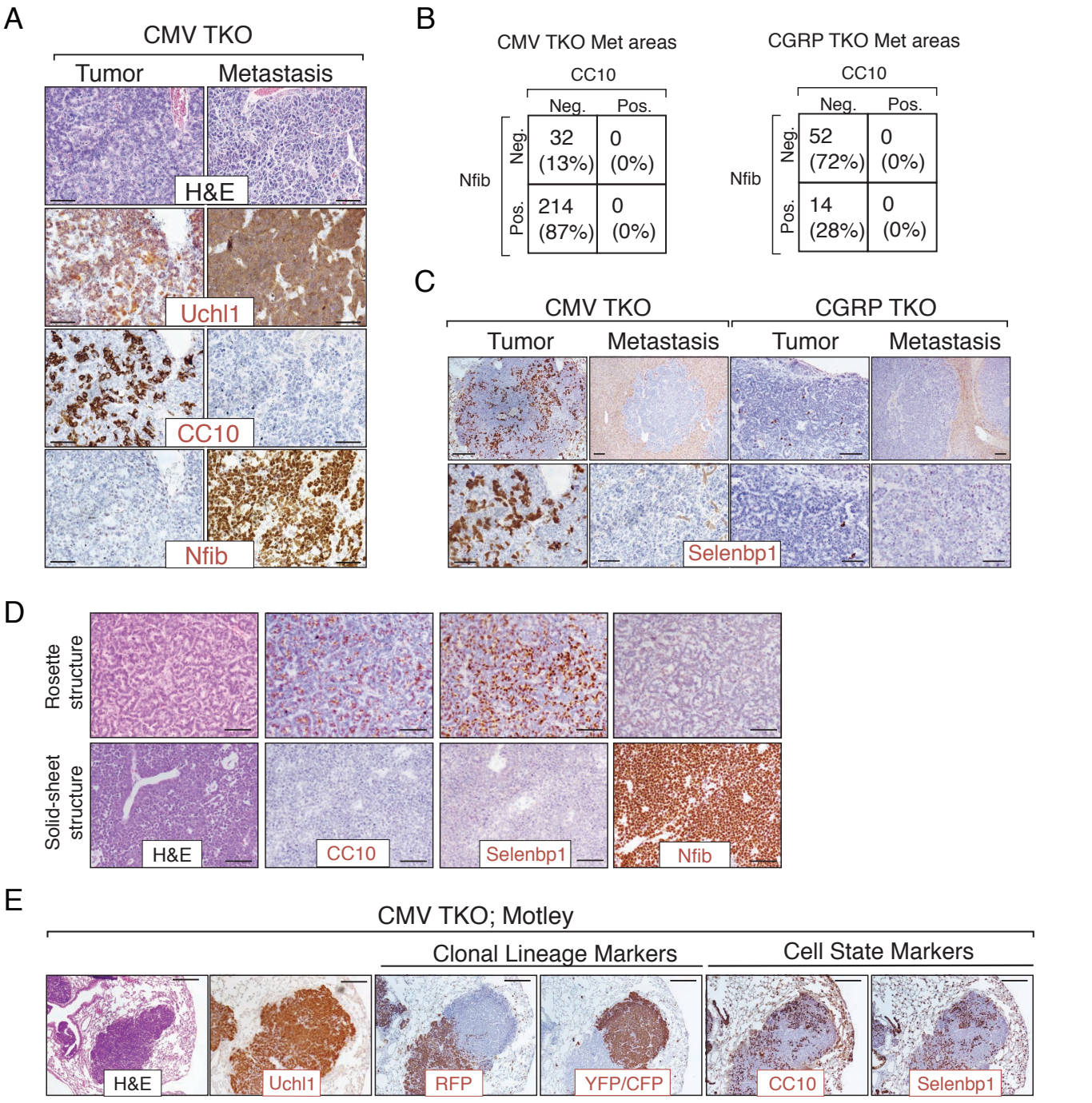

Figure S13: Multilineage differentiation in CMV TKO Nfib^{low} primary tumors.
A-B. Immunohistochemical staining and quantification of CC10 and Selenbp1 of mouse SCLC tumor sections. Scale bars = 50 μm. Quantification of tumor state/subtype marker expression $P < 0.0001$ (one way ANOVA).
C. Immunohistochemical staining for Nfib and Selenbp1 in primary tumors and metastases from CMV TKO and CGRP TKO mice. Scale bar top = 100 μm, bottom = 50μm.
D. Immunohistochemical analysis for CC10, Selenbp1, and Nfib in rosette and solid-sheet structures of primary tumors from CMV TKO mice. Scale bars = 50μm.
E. Immunohistochemical staining of tumor lineage markers (RFP, YFP/CFP) and SCLC non-metastatic markers (CC10, Selenbp1) in tumor from CMV TKO;Motley mice. The unique staining of tumor lineage markers in each individual tumor suggests each tumor from the CMV TKO model is clonal. Scgb1a1^{positive} and Selenbp1^{positive} sub-populations expression cells are cancer cells and are clonally derived. Scale bars top = 200μm.

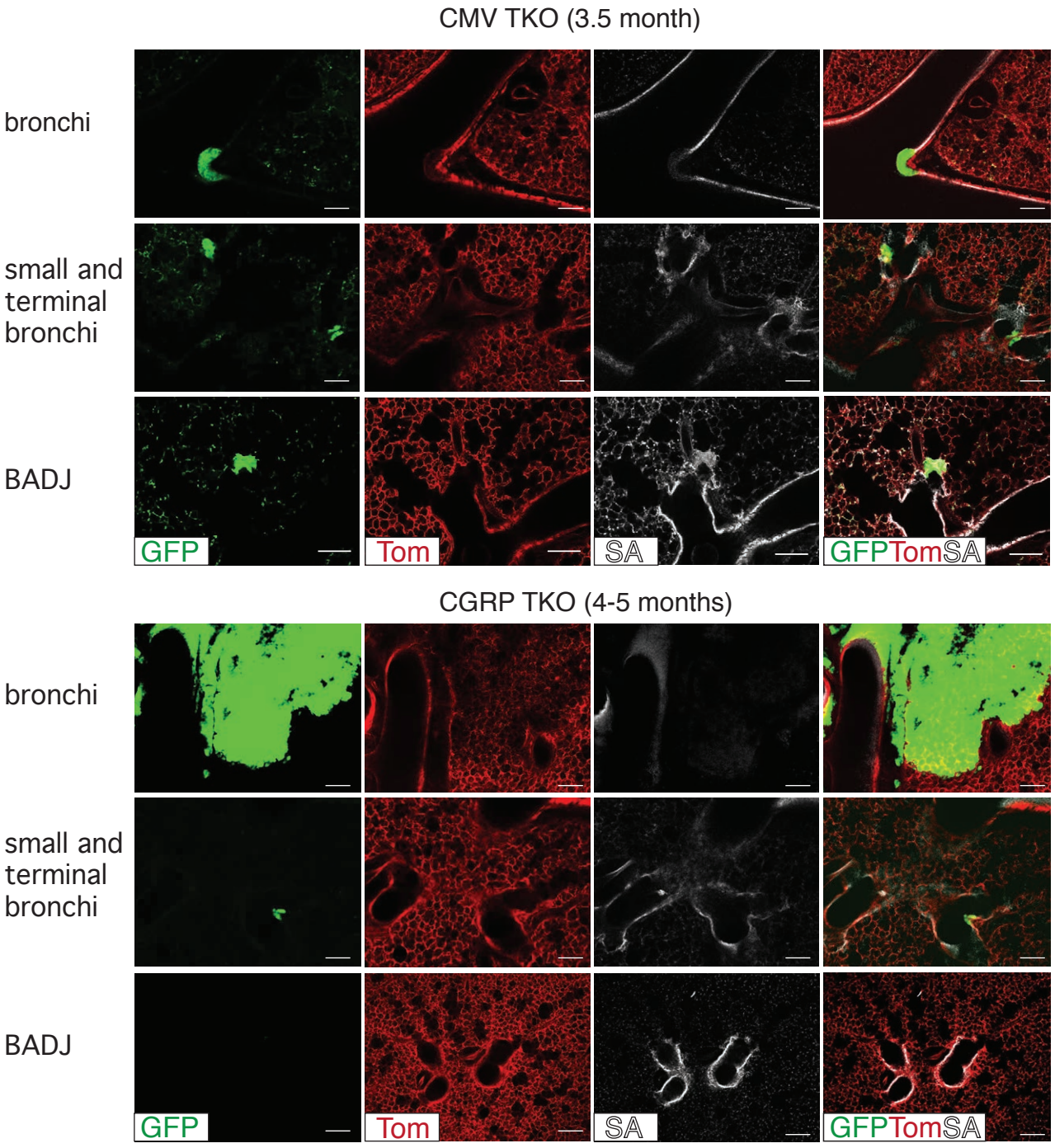

Figure S14: SCLC lesions in CMV TKO and CGRP TKO mice have different location distributions. Confocal wholemount imaging of CMV TKO and CGRP TKO lesions (Tumor lesions: GFP, Normal lung: RFP, streptavidin staining labels lung epithelium). Individual channel from the images in Figure 6A are shown. Scale bars = 200μm.

A

Cohort	Titer	Virus Type	Conclusions
CMV-Cre	8 x 10^8	Ad-CMV-Cre	Mice develope large numbers of SCLC.
CGRP-Cre	8 x 10^8	Ad-CGRP-Cre	Mice develop ~50-fold fewer SCLCs than CMV-Cre TKO mice. Not the major cell-type of origin
CC10-Cre	8 x 10^8	Ad-CC10-Cre	Not a cell-type of origin of SCLC
SPC-Cre	8 x 10^8	Ad-SPC-Cre	Mice develop very few SCLC. Not a major cell-type of origin
CGRP-Cre +CC10-Cre	4 x 10^8 4 x 10^8	Ad-CGRP-Cre Ad-CC10-Cre	No obvious non-cell-autonomous effect on promoting CGRP-Cre driven SCLC
CGRP-Cre +CC10-Cre +SPC-Cre	2.6 x 10^8 2.6 x 10^8 2.6 x 10^8	Ad-CGRP-Cre Ad-CC10-Cre Ad-SPC-Cre	No obvious non-cell-autonomous effect on promoting CGRP-Cre driven SCLC

B

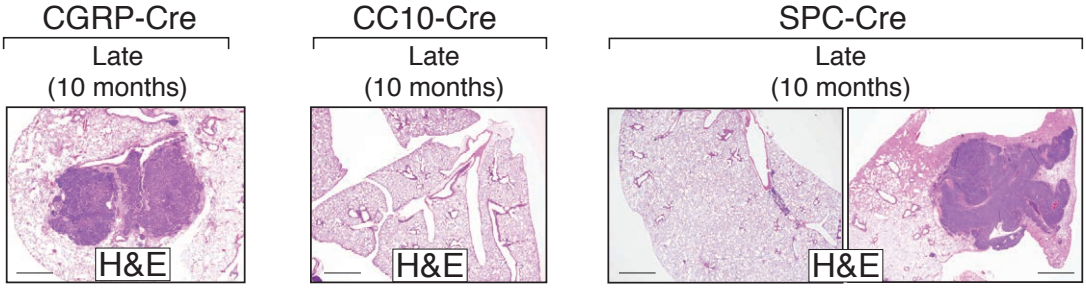

C

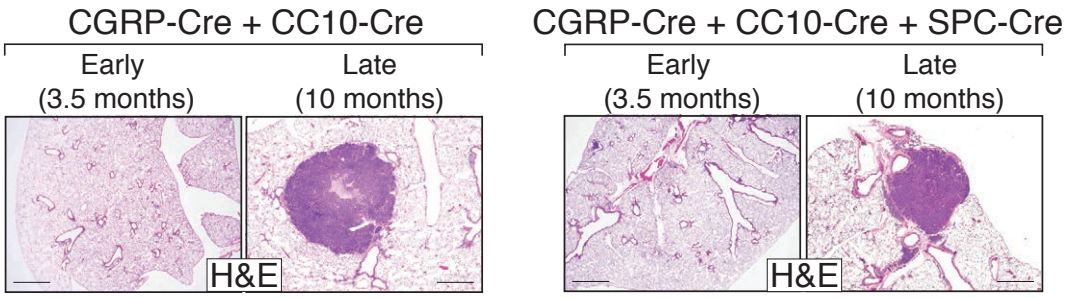

Figure S15: Ad-SPC-Cre and Ad-CC10-Cre induce no/few SCLC tumors in TKO mice.
A. Summary of different cohorts of *TKO;mTmG* mice transduced by adenoviral vectors with different tissue-specific promoters driving Cre expression. Virus type and titer are specified for each group. None of single or combined virus with tissue specific promoters driven Cre expression can recapitulate the efficiency of Ad-CMV-Cre in driving SCLC tumorigenesis. At this titer, *TKO;mTmG* mice transduced with Ad-CMV-Cre need to be euthanized due to their tumor burden 4-5 months after tumor initiation (hence that lack of a 10 month CMV-Cre cohort in Figure 6C).
B-C. H&E staining of lung from *TKO;mTmG* mice transduced with adenoviral vectors with different tissue-specific promoters driving Cre expression. Representative sections of the lungs of mice transduced with Ad-CGRP-Cre, Ad-CC10-Cre and Ad-SPC-Cre 10 months after transduction are shown (**B**). Representative sections of the lungs of mice transduced with a combination of Ad-CGRP-Cre and Ad-CC10-Cre or a combination of Ad-CGRP-Cre, Ad-CC10-Cre and Ad-SPC-Cre 3.5 and 10 months after tumor initiation are shown (**C**). Scale bars = 1 mm.

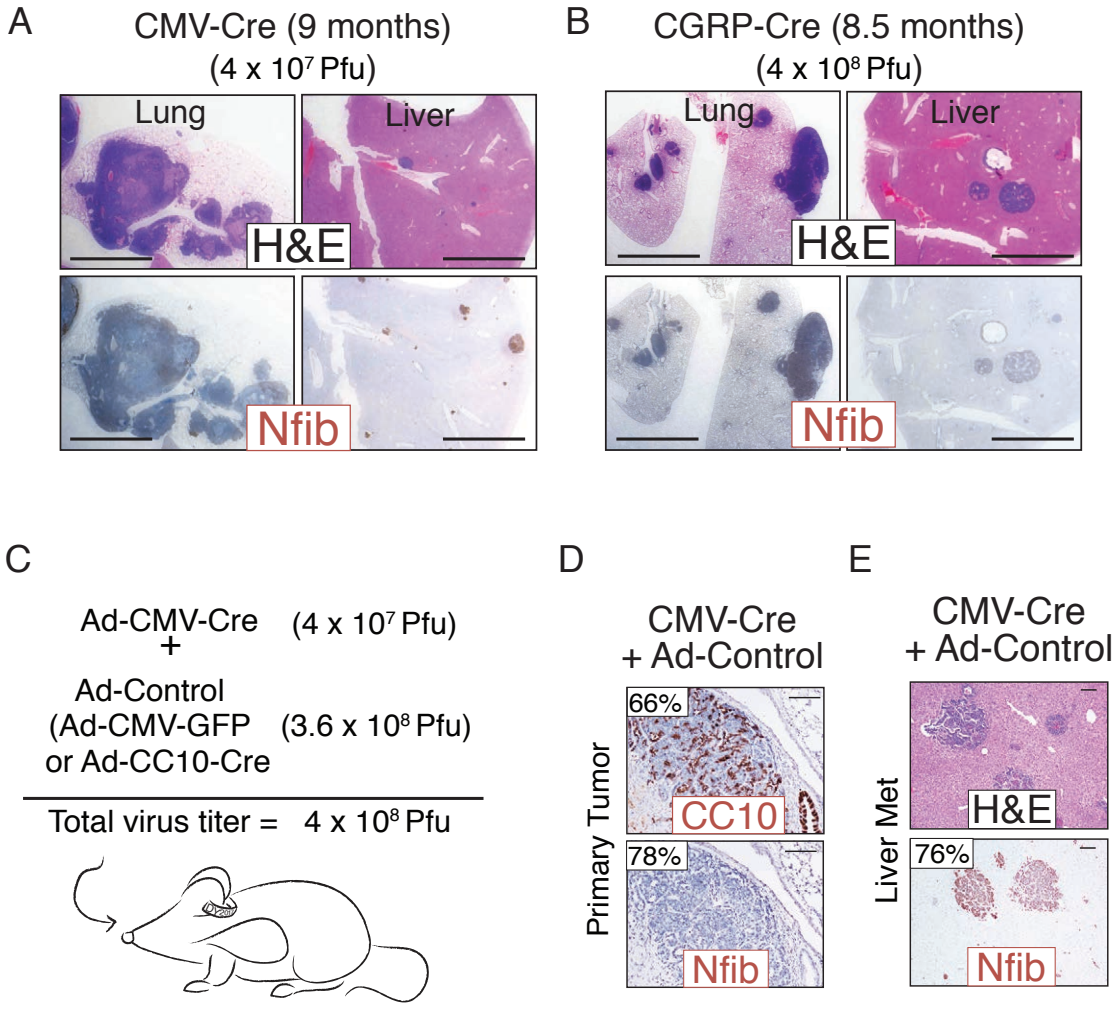

Figure S16: Nfib-negative tumor progression in CGRP TKO mice is not driven by the time after tumor initiation or any non-specific effect of the higher viral titer used to initiated tumor Ad-CGRP-Cre
A-B. H&E and Nfib immunohistochemistry of lung tumors and liver metastases harvested from CMV TKO **(A)** and CGRP TKO **(B)** mice that were aged for a very similar amount of time. These data suggest that time of aging does not play a role in Nfib-negative tumor progression in CGRP TKO mice. Scale bars = 2mm. Note that the CGRP TKO mouse received 10-fold more virus.
C. Schematic image showing mice transduced with Ad-CMV-Cre in combination with control virus (Ad-CMV-GFP or Ad-CC10-Cre) such that the mice got the equivalent total amount of adenovirus as mice transduced with Ad-CGRP-Cre. This experiment was set up to test whether any non-specific effect(s) of the higher total amount of adenovirus impacts whether primary SCLCs express multilineage markers and whether they gain Nfib expression during metastatic progression.
D-E. Representative H&E and Nfib immunohistochemistry of a primary tumor (**D**) and liver metastases (**E**) from mice in which tumors were initiated with Ad-CMV-Cre (4 x 10^7 Pfu) combined with Ad-Control (3.6 x 10^8 Pfu of either Ad-CMV-GFP or Ad-CC10-Cre) such that the mice were transduced with a titer of virus comparable to that used for CGRP TKO mice (4 x 10^8 Pfu). Percent of primary tumors that contain $CC10^{positive}$ cells and the percent of metastases that are $Nfib^{high}$ are indicated. Scale bars = 100 μm.

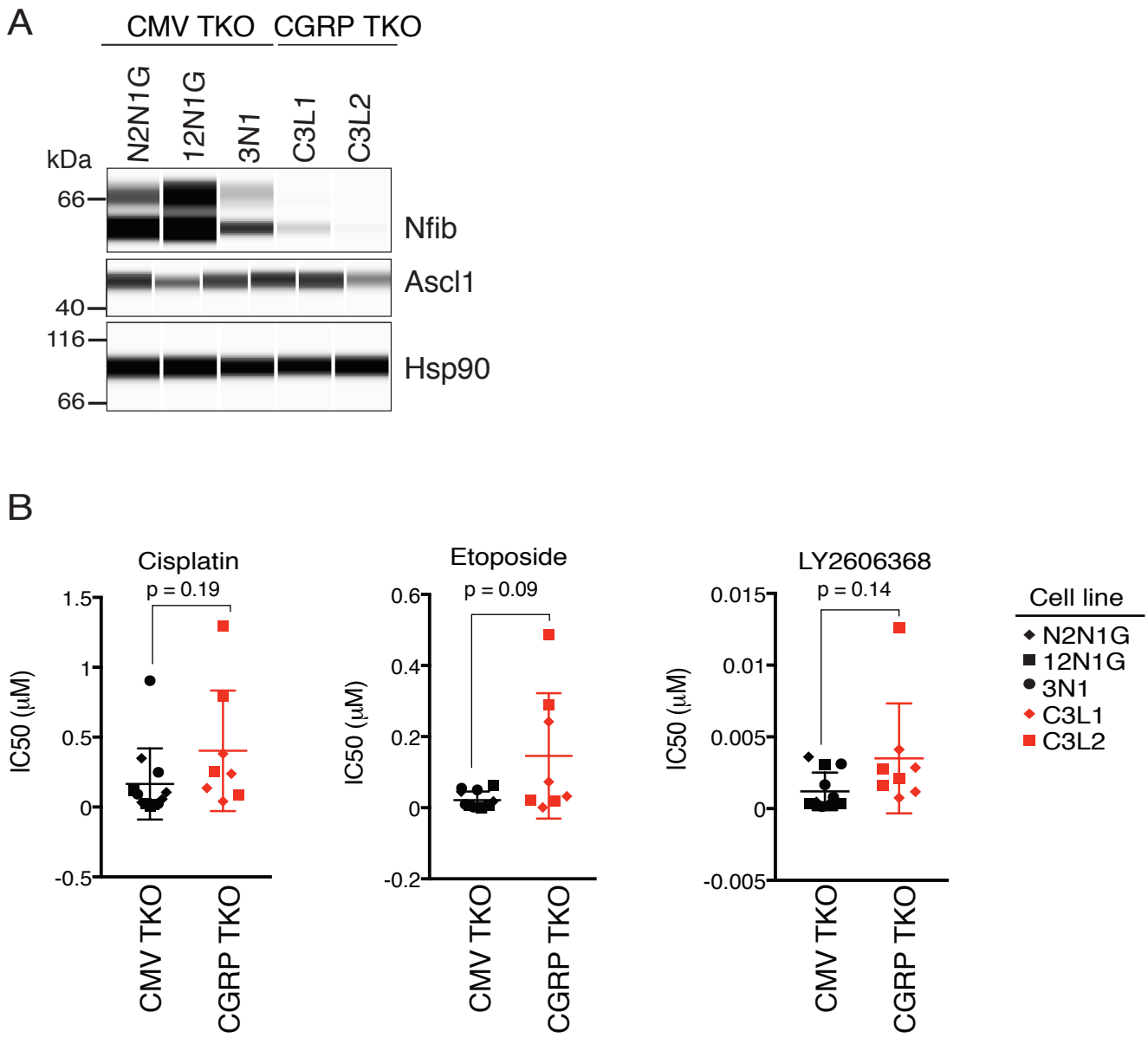

Figure S17. CMV-TKO and CGRP-TKO cell line have similar responses to therapies.
A. Nfib protein expression in 3 CMV TKO cell lines and 2 CGRP TKO cells lines. All CMV TKO cell lines have high Nfib expression, while all CGRP TKO cell lines are Nfib low. All cell lines express Ascl1 consistent with the neuroendocrine nature of these lines. Hsp90 shows loading.
B. CMV TKO and CGRP TKO cell lines have similar responses to cisplatin, etoposide, and Chk1 inhibitor (LY2606368). Each symbol is one replicate of each cell line (n = 4 replicates per cell line), with each cell line represented by a different symbol. Bars are the mean and error bars are the standard deviation.